

We are IntechOpen, the world's leading publisher of Open Access books Built by scientists, for scientists

6,900

Open access books available

186,000

International authors and editors

200M

Downloads

Our authors are among the

154

Countries delivered to

TOP 1%

most cited scientists

12.2%

Contributors from top 500 universities



WEB OF SCIENCE™

Selection of our books indexed in the Book Citation Index
in Web of Science™ Core Collection (BKCI)

Interested in publishing with us?
Contact book.department@intechopen.com

Numbers displayed above are based on latest data collected.
For more information visit www.intechopen.com



Rotation Invariant on Harris Interest Points for Exposing Image Region Duplication Forgery

Haitham Hasan Badi, Bassam Sabbri and Fitian Ajeel

Additional information is available at the end of the chapter

<http://dx.doi.org/10.5772/intechopen.76332>

Abstract

Nowadays, image forgery has become common because only an editing package software and a digital camera are required to counterfeit an image. Various fraud detection systems have been developed in accordance with the requirements of numerous applications and to address different types of image forgery. However, image fraud detection is a complicated process given that is necessary to identify the image processing tools used to counterfeit an image. Here, we describe recent developments in image fraud detection. Conventional techniques for detecting duplication forgeries have difficulty in detecting postprocessing falsification, such as grading and joint photographic expert group compression. This study proposes an algorithm that detects image falsification on the basis of Hessian features.

Keywords: copy-move detecting, doubled region, Harris pursuit point

1. Introduction

Brain-computer interface (BCI) technology provides a means of communication that allows individuals with severely impaired movement to communicate with assistive devices using the electroencephalogram (EEG) or other brain signals. The practicality of a BCI has been made by advances in multi-disciplinary areas of research related to neuroscience, brain-imaging techniques and human-computer interfaces. The end goal of a BCI is to enable monitoring of the underlying brain processes and subsequent utilization of this information for communicating and controlling devices solely through the brain without depending on the normal output pathways of peripheral nerves and muscles. Photographs capture reality. However, this belief no longer holds true in the current digital era given that the

manufacture of counterfeit images has increased [1]. The development of powerful photo editing software, such as Photoshop, has simplified the production of fake digital images [2]. A case of image counterfeiting is shown in **Figure 1**. Image forgery has severe consequences. For example, by modifying faces in an image, image counterfeiting can be applied to ruin a person's reputation. Academic documents may also include manipulated images that misrepresent experimental data. In addition, image forgery can be applied to remove a reference object from a standard image. As a result, the validity of the image can no longer be accepted [3]. These multilevel protection issues have different implications in different fields, such as detective work.

In simple terms, a brain-computer interface (BCI) is a direct interface between the human brain and an artificial system. Its purpose is to control the actuation of a device, say a robotic system or a wheelchair, with brain activity but without the use of peripheral nerves or muscles [4]. BCI in a literal sense means interfacing an individual's electrophysiological signals with a computer [5]. Thus, in a true sense, the BCI only uses signals from the brain and must consider eye and muscle movements as artifacts¹ or noise. Information from various knowledge domains is necessary to create a complete BCI system. Thus, an artificial neural network (ANN) is an information-processing paradigm that is inspired by the way in which biological nervous systems, such as the brain, process information. This network is composed of a large number of highly interconnected processing elements referred to as neurons that work in unison to solve specific problems. Enhancing the noisy electroencephalogram (EEG) signal utilizes a layer of neurons in the spatial dimension within the neural network framework. The incoming noisy input signal sample is treated as a probability density function (pdf) by the layer of neurons and it recurrently evolves under the influence of the SWE and appropriate learning rules. This approach has made possible the development of an efficient computational algorithm referred to as the recurrent quantum neural network algorithm (RQNN) which to some extent has solved the complex problem under consideration. In general, two methods can be applied to detect image fraud: active and passive certification [6]. These two methods are illustrated in **Figure 2**. Active certification is categorized into two classes. The first class is based on the identification of a digital watermark. A watermark is hidden in the image at the end of capture, the detection program checks if the image certificate has been edited [7, 8]. The watermark is inserted when the image is taken using a specially equipped photographic camera or after acquisition by an expert [1]. The successive editing

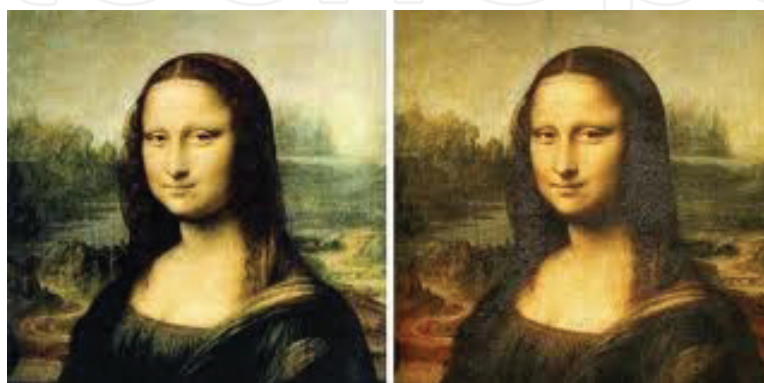


Figure 1. Image forgery has severe consequences.



Figure 2. Detect image fraud: active and passive certification.

of the original image may degrade image quality. Passive certification methods are based on digital signatures. These methods identify the distinguishing characteristics of an image as a signature after image acquisition. At the end of certification, signatures are renewed in accordance with a similar method, and the genuineness of the image can be identified by comparison. Digital signatures and watermarks have similar disadvantages. Negative image certification, also referred to as forensic digital image certification, is highly practical. Digital image certification does not require extra information and is independent of the image theme [9]. Negative methods have two parts: (1) identification of the original edit and (2) detection of tampering [10]. Certification for the first class is based on digital fingerprint certification, effects allowed by image acquisition, and storage. The methods used in this class use the digital fingerprint of the camera to differentiate among similar or dissimilar camera models. The detection methods of passive falsification can either be false or independent. Fraud detection methods are employed in particular cases of counterfeiting, similar to making copies or linking images. To discover universal forgery, researchers use autonomous techniques and exploit three different types of artifacts: the effects of resampling, pressure, and contradictions [10]. The types of counterfeiting techniques can be categorized into two classes: copy-detecting technique (image forging) and image-binding technique (two-fold image-based counterfeiting).

2. Copy-move forgery detecting

The ease and effectiveness of counterfeiting facilitates its application in changing image content [11]. The important features, like the pallet and the active range, of replicated areas are compatible with the rest of the image given that these areas are obtained from the same image [12]. Nevertheless, in practice, counterfeiting may imply more than simple replication. Numerous image-editing processes may be applied in serious counterfeiting, as shown in **Figure 3**. The processes can be divided into two groups: intermediary processes and post-processes. Intermediator processes are applied to synchronicity and homogeneity between a replicated region and its neighbor [13]. Intermediator processes include rotation, scaling,

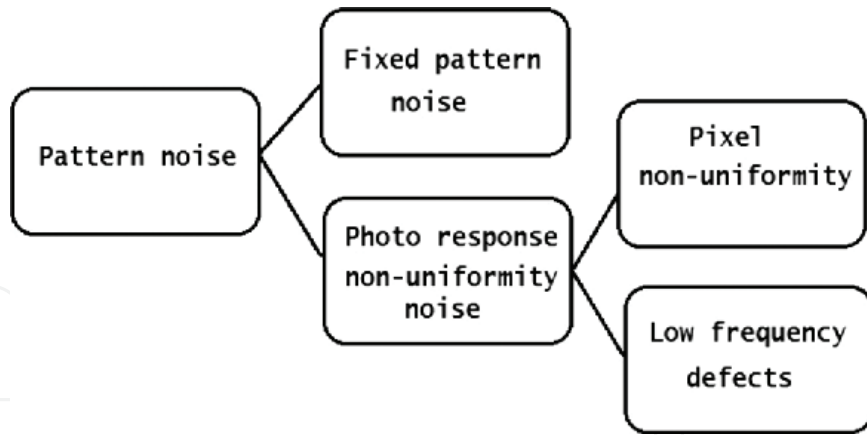


Figure 3. Image processing operations associated with image forgery.

reflection, lighting adjustment, or color adjustment. In serious cases, intermediary processes can be combined. Postprocesses, such as noise addition, joint photographic expert group (JPEG) compression, or blurring, can be applied to delete all retraces that can be detected in the copy process, such as sharp edges [2]. A broad range of easily available algorithms has been proposed to detect replicated images and functions, as shown in Figure 4.

To detect image forgery, an image is first selected (e.g., converted to gray scale). The image is divided into an auction block of nested pixels. The size of the image m_n , size of block B , and the number of overlapping blocks is given by:

$$\text{No of blocks} = (m - k + 1) \times (n - k + 1) \tag{1}$$

The vector is an extractable characteristic in each block. The vector-matching function is highly similar to pairing functions. Known pairing methods include the arrangement of miracle dictionaries on the element vectors and the identification of the nearest neighbor in the tree Kd . The similarity between two attributes can be determined on the basis of similarities between different parameters, such as Euclidean length. In the verification step, extreme values are suppressed and holes are filled up through a basic filtration step, such as morphing.

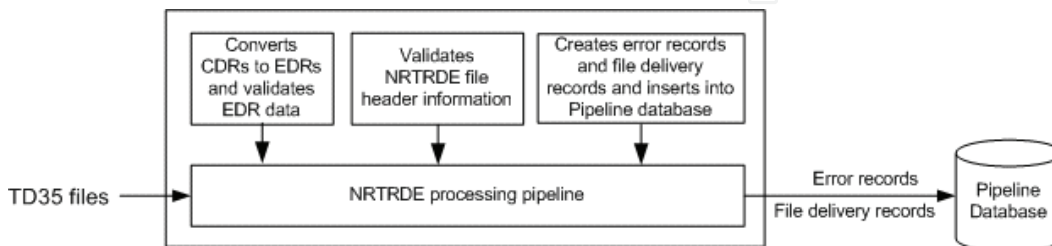


Figure 4. Pipeline of a fraud detection algorithm.

3. Copy-move detecting algorithm

Numerous articles on the negative detection of displacement in images have been and continue to be published. Existing methods for displacement detection are primarily distinguished on the basis of the case and sizing of the function applied to match the image block. This article classifies existing methods in accordance with the extracted properties applied to test block similarities. In the following sections, different cases or classes of detection algorithms are presented.

3.1. Algorithm based on invariant keypoints

In contrast to other algorithms, this algorithm does not divide the image into auction blocks to extract features but instead extracts features from the intact image. Feature extraction is performed with SIFT and speeded-up robust feature (SURF). This technique is applied to derive the characteristic local feature of an image and produce a keypoint in accordance with preset requirements. The vector sum/descry values are fixed for rotational, translational, and scale measurements and are partially fixed for strong illumination changes in local geometric distortion [14, 15]. The first attempt to exploit this algorithm was reported by [16]. In the algorithms, only the correspondence of the keypoint can be achieved by its maximum bin, including the identity of the nearest neighbor [17]. SIFT has been adopted to identify replicated regions in a counterfeit image. The SIFT signifier is applied to detect copied areas by coping with keypoints rather than clusters. This algorithm has excellent detection accuracy but otherwise poor performance.

3.1.1. SIFT algorithm

He proposed the SIFT algorithm, which could be used to detect and evaluate the geometrical shifts applied to forged displacement copy-and-paste images. The detection procedure involves three steps: In the first step, SIFT functions are extracted and main points are associated. The second step is committed to keypoint compilation and fraud detection. The third step estimates the engineering shifts, if any, that occurred. SIFT can be executed under the conditions of eminent real rate (TPR) and abject fake positive degree ratio (FRE), JPEG compression, and additional noise. In addition, SIFT can accurately estimate different arguments for affine transmutation. **Figure 5** shows different arguments for affine transmutation.

The first attempts to take advantage of SIFT have been reported in [16]. In SIFT, the correspondence of the key indicator is achieved by first identifying the neighbor closest to the best bin [17]. SIFT has been adopted to identify a single copy in the counterfeit image. SIFT descriptors are usually applied to identify keypoints of copied areas instead of blocks, whereas other algorithms cope with object indicators. Although SIFT exhibits excellent detection performance, its false-positive rate remains unknown. In [18], the main SIFT points were extracted from the image and were then associated to obtain the corresponding keypoints. A vote scheme based on vector direction was applied to distinguish between origin and direction. Then, an

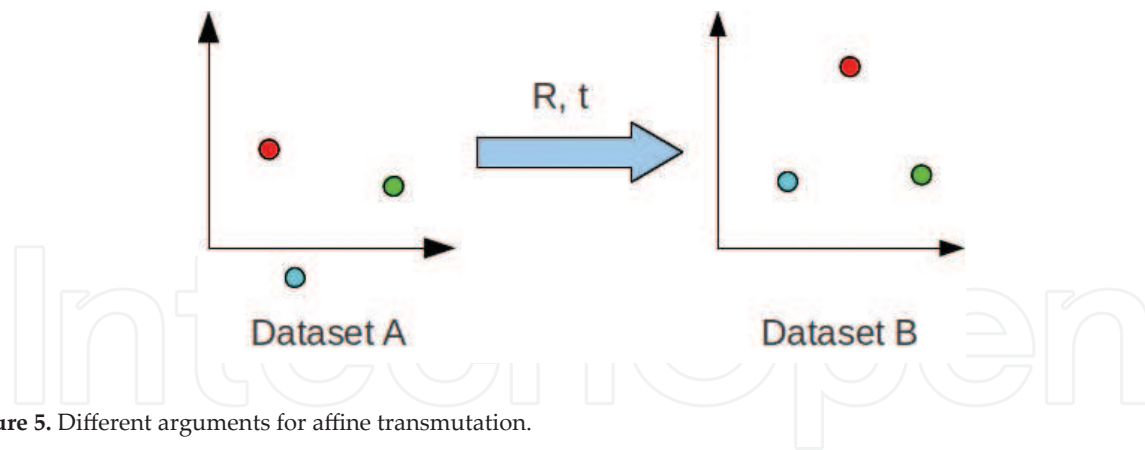


Figure 5. Different arguments for affine transmutation.

efficient two-fold sub-window search algorithm (EES) was used to locate duplicated areas within the border box. Finally, a pixelwise partition was identified. The experiment solutions demonstrated that the proposed algorithm remains robust even with background noise and engineering manipulation [19]. He suggested a SIFT algorithm that could detect and then estimate the geometrical transformation applied to forge displacement copy-and-paste images. The detection process involves three steps. In the first step, the SIFT function is extracted and corresponding keypoints are identified. The second step involves the consolidation and detection of fraud. The third step identifies changes that occurred. SIFT has high positive identification rate and low false positive rate even under JPEG image compression and added noise conditions. In addition, it accurately estimates several affine transformation parameters. Refs. [20, 21] suggested a SIFT-established detecting algorithm that can be used to estimate the geometrical transformation applied to the copy. The algorithm begins by converting the suspected image into grayscale. SIFT is then applied to collect image characteristics for the detection of keypoint sources. In SIFT, the keypoint sources are initially adapted in accordance with the characteristics of the vector sum used in the better bin-first algorithms. The potential geomagnetic distortion of the refined areas is estimated on the basis of the assumed paired keypoints by applying RANSACK. SIFT is more robust than intermediary processes even when JPEG compression or noise are added to the processed image. Furthermore, affine transformation is exactly estimated, particularly in larger duplicated areas. A different scenario is to integrate SIFT into copy detection systems [22]. Instead of applying SIFT to detect keypoints, the Harris quicker from SIFT is applied. After all keypoints are revealed, SIFT is applied to generate the descriptive characteristics of extracted features. Then, the Kd trees algorithms are applied to match the keypoints to identify duplicated areas. The algorithms can effectively detect copied areas, such as unrotated scanlines or Gaussian noise conditions, that have undergone transformation [5, 22]. Harris detection, which is quicker than SIFT, has been used to detect keypoints. After keypoint detection, SIFT is applied to identify a unique characteristic from extracted keypoints. The Kd tree algorithm is then applied to match keypoints to determine duplicate areas. This algorithm can efficiently detect areas, such as scanlines, that have undergone transformation.

3.1.2. SURF algorithm

SURF has been adopted to detect image editing processes, such as rotation and gradation. SURF is superior to SIFT in detecting image strengths and performs as well as SIFT. The

complicated automatic reinstallation of duplicate areas hinders the practical applications of these algorithms. We propose a novel algorithm for the detection and description of scale and constant rotation in images. The algorithm is based on SURF and thus has powerful acceleration functions. SURF approximates or even exceeds the proposed thresholds for redundancy, excellence, and sustainability and rapidly performs calculation and comparison. This operation is performed by relying on image confluence. The exit detection and prescriptive prescriptions are based on their strengths (if a Hessian scale is used to detect and describe the established distribution), and kernel methods are simplified to allow the combination of new detection, description, and correspondence. Correspondence between two images of the same view and the objective is partly achieved by using many computers. In this study, photography, three-dimensional reconstruction, image recording, and objective recoding were conducted. The search for a separate image match—the purpose of our research—can be separated into three principal steps. First, points of interest are specified in the characteristic locations of the image, such as angles, points, and plus T-intersections. The most important property of a detection method is its repeatability, that is, its reliability in finding similar indicators of interest under different conditions. Then, each point of interest is represented by a transmitter characteristic. This description must be distinct and must have similar time strengths under noise conditions, mistake detection, and geometrical and photometrical distortions. Finally, vector descriptors are adapted in different images. Correspondence is based on vector distance. Descriptor size directly affects computational time. Thus, fewer dimensions are desired. We aimed to develop an algorithm for the detection and the identification of fraud. We compared the performance of our proposed algorithm with that of a state-of-the-art detection algorithm. Our algorithm exhibits computational time and robust performance. Downsizing after description and complexity must be balanced while providing sufficient distinction. Various detection and description algorithms have been proposed in the literature (e.g., [1–3, 6, 7, 23]). Furthermore, detailed datasets for comparison and standard assessment have been established [8–10]. We build upon the knowledge gained from previous work to better understand the aspects that contribute to algorithm performance. When used in experiments on standard image sets, as well in the application of actual objective recognition, the algorithm exhibited rapid detection and description, as well as distinctive and reproducible performance. While working with local features, stability is the first issue that requires resolution and depends on the expectation of geometrical and photometrical distortions. This turn of events is identified by the possibility changing in conditioning. We concentrate on the detectors and constant descriptions of the balance and rotation of the image. These detectors offer better compromises among the complexity of the functionality and the durability of the distortions that usually occur. The discrepancy and gradient of anomalies and the effects of perspective are secondary to the effect covered by the overall durability of the description [2]. The additional complexity of affine invariance negatively affects sustainability, unless significant changes are anticipated. In some cases, even analog rotation can be abandoned with solutions in a fixed static version of our description. We refer to this ability as “erect SURF” (U-SURF). In fact, in some applications, such as cell robotic navigation or visual guidance, the camera often only revolves around the vertex. Taking advantage of avoidance of the exaggerated stability of rotation in similar events not only increases speed but also increases discriminatory force. As for the photometric, we assumed a simple linear accelerator example with a scaled factor and displacement. Note that our detection and description do not apply color.

4. Related work

The most commonly used detection method is the Harris-cornered method [24], which was proposed in 1988. It is based on the intrinsic values of the secondary-momentary matrix. However, Harris angles are not fixed. The Lindberg detection method introduces the principle of automatic scaled selection [1], which allows the detection of a full point of interest in an image together with its scope. He experimented with the Hessian matrix operation identifier and Laplacian (corresponding to the Hessian matrix operation effect) to detect bulb structure. The detectors, which were developed by Harris-Laplace and Hessian-Laplace, are robust and stable with high reproducibility [25]. The Harris (Adaptive Scale) or the Hessian Matrix Locator and Laplacian have been applied to determine scale. Focusing on speed, [26] estimates Laplace Gaussians (LoG) on the basis of the candidate Gauss (DoG). Several fixed-interest rate detectors that increase the entropy in the area and the edged-based zone detection have been proposed [11]. Nevertheless, these detectors are inflexible. Several detection methods have been proposed for fixed properties that can adapt to long-term changes but are not discussed in this article. A review of the literature [9, 12] shows that (1) Harris-based detection methods are stable and replicable. The use of a specific Hessian matrix addition instead of its effect (the Laplacians) is useful because fires occur less on elongated and nonlocal structures. In addition, (2) an approximation, such as DoG, has low-cost computational speed and low loss of precision. A wider set of attribute descriptions has been suggested, such as the Gaussian-derived function [13], a fixed moment [27], complex feature [4, 28], guiding filters [29], and phase-localized functions [30], to represent the distribution of small features in a region of interest. The latter [2] has been shown to surpass the others [8] because they capture a basic quantity of information on the special intensity of level models when large to small deformations or localization mistakes occur. In [2], SIFT has been applied as a general level gradient diagram around the indicator of interest and is stored in boxes in a 128-dimension vector (eight routing boxes for each 4×4 box). Various improvements have been proposed on this basic scheme [3]. PCA has been applied to slope images. These operations (PCA, SIFT) provide a 36-dimension characteristic that is rapidly harmonized but is less distinct from SIFT in terms of secondary comparison [9]. The slow calculation function reduces the impact of quick coping. In similar papers [9], the authors suggested a variation on SIFT, named GLOH, which proved to be more distinct with the same dimensional count. However, GLOH is computationally expensive. SIFT is the most attractive for practical application and is currently the most widely applied algorithm. It is distinct and relatively quick, which is crucial for online applications. Recently, [31] used a field-programmable area grid to improve its order of magnitude relation. However, the height dimensions of the descriptions in SIFT are defective when compared with those of corresponding methods. For online applications on an ordinary computer, each of the three steps (detection, description, and correspondence) must be fast. Alternatively, best-bin-first [2] accelerates computation but provides inaccurate solutions. A novel detection method based on SURF has been proposed by [1, 25]. However, basic approximation was applied because DoG [2] is a basic Laplacian-based detector. Given that it depends on the embedded image to reduce computing time, we designated this algorithm as the "Quick Hessian" detector. Description, on the other hand, describes the distribution of the Haar-wavelength reactions in the area of interest. We operate the built-in speed images repeatedly. In addition, only 64

dimensions are used, thus decreasing the calculation time of the corresponding characteristic and simultaneously increasing durability. We again propose a new index step based on the Laplacian marker. This step accelerates correspondence and increases the robustness of the description. To illustrate the self-sufficiency of the algorithm, we briefly discussed the conception of an integrated image, as defined in [32]. It allows the quick execution of filter to wrap a box type. The insertion of an integrated image $I_{\Sigma}(z)$ into $x = (z, y)$ represents the amount of all the pixels of the income I of a rectangularity area formed by the z and the origin.

$$I_{\Sigma}(\mathbf{x}) = \sum_{i=0}^{i \leq x} \sum_{j=0}^{j \leq y} I(i, j) \quad (2)$$

The calculated I_{Σ} only requires four additions to calculate the total intensity on any vertical and rectangular surface, regardless of its shape.

5. Quick-Hessian detection

We based our detection method on Hessian matrix addition because of its superior calculation time and accuracy. Therefore, instead of using an applied range to select position and scale (as in the Hessian-Laplace [25]), we used a Hessian identifier for both. Given the indicators $z = (z, y)$ in **Figure 1**, the matrix Hessian $H(z, \sigma)$ in x is defined on the scale as follows.

$$\mathcal{H}(\mathbf{x}, \sigma) = \begin{bmatrix} L_{xx}(\mathbf{x}, \sigma) & L_{xy}(\mathbf{x}, \sigma) \\ L_{xy}(\mathbf{x}, \sigma) & L_{yy}(\mathbf{x}, \sigma) \end{bmatrix}, \quad (3)$$

where, similar to $L_{zy}(z, \sigma)$ and $L_{yy}(z, \sigma)$, $L_{zz}(z, \sigma)$ is the rotation of the Gaussian second-order differential $\partial^2 \partial z^2 g(\sigma)$ with the image I in indicator z . Gaussian analysis has been optimized for large-scale analysis, as shown in [33]. However, in practice, Gaussian analysis should be reduced (**Figure 1** of the allowed half) because filtering Gaussians with aliases will result in image subsamples. In addition, a property that cannot show new structures when resolutions are decreased has been proven in one-dimensional images and cannot be applied in two-dimensional images [34]. Thus, the importance of the Gaussian filter may have been exaggerated in this respect, and here we test a simple alternation. Given that the Gaussian filter is not idealistic in any event because of the success of the LoG with the approximations of the newspaper, we push the rounding with the filters of the box (**Figure 6** on the right). These approximate Gaussian second-class derivatives can be rapidly evaluated with an integrated image irrespective of size. It can be evaluated very quickly using embedded images regardless of size. The algorithm's performance is similar to that used for esterized crops and Gaussians.

When applied to rectangular areas, SURF remains simple and arithmetically efficient. However, we need additional relative weight in equilibrium. This weight is specifically expressed with

$$\frac{|L_{xy}(1.2)|_F |D_{xx}(9)|_F}{|L_{xx}(1.2)|_F |D_{xy}(9)|_F} = 0.912... \simeq 0.9, \quad (4)$$

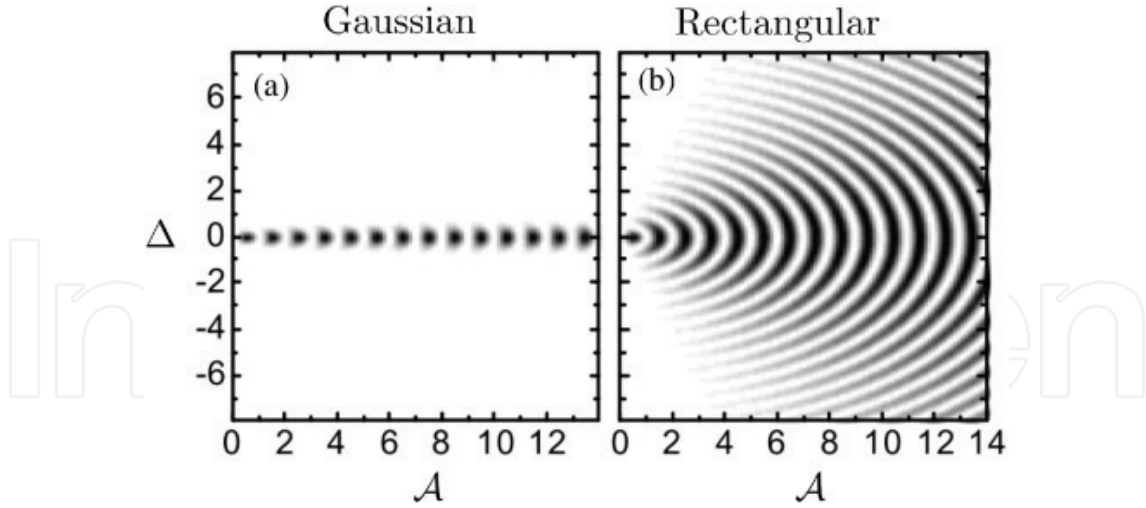


Figure 6. Left to right: (intact and trimmed) Gaussian secondary arrangement partly derived in the y -direction and zy -direction, and our approximation of the applied box filter. Gray areas are null.

where $\|z\|_F$ is the Frobenius norm.

$$\text{let}(\mathcal{H}_{\text{approx}}) = D_{xx}D_{yy} - (0.9D_{xy})^2. \quad (5)$$

In addition, the responses to the filters are normalized to mask size to ensure that the continuous Frobenius is standard for any filter size. In an image, space generally takes the form of a triangle. The image is repeated with a Gaussian filter and subsamples to reach the apex of the triangle. Given the application of box filter and plot image, we do not duplicate the filtering to output a previous filter layer. Nevertheless, filters of any size can be used at the same speeds when applied to the original image (even parallel to the latitude, if not used here). Therefore, size spacing is analyzed by increasing filter size rather than decreasing image size. The output of the 9×9 filters above is considered as the primary gauge level. Thus, scaling $s = 1.20$ (corresponding to the derivate Gaussian with $\sigma = 1.20$). The following levels are obtained by filtering the image with a progressively larger mask, taking into account the distinct nature of the integrated image and the specific structure of our filter. Specifically, this phenomenon leads to sizes 9×9 , 15×15 , 21×21 , and 27×27 . On a large scale, the increment in filter size must also vary accordingly. Thus, for each new Octavian, the volume of the filter doubles from 6 to 12 to 24. At the same time, sampling periods can be doubled to enable the extraction of points of interest. Given that our filter arrangement ratios remain constant after expansion, the bypass scale is approximately matched. For example, 27×27 filters correspond to $\sigma = 3 \times 1$, $2 = 3$, $6 = s$. Moreover, given that the Frobenius base remains constant in our filtering, they soon normalize [35]. To locate points of interest in the image and the scaling, maximizing suppression is not applied on the $3 \times 3 \times 3$ neighbor. The maximum limit for the Hessian matrix is then encountered in the range and proposed spacing of the image [36]. The spatial interpolation scale is particularly important in our case, and the difference in size among the first levels of each Octavian is relatively large.

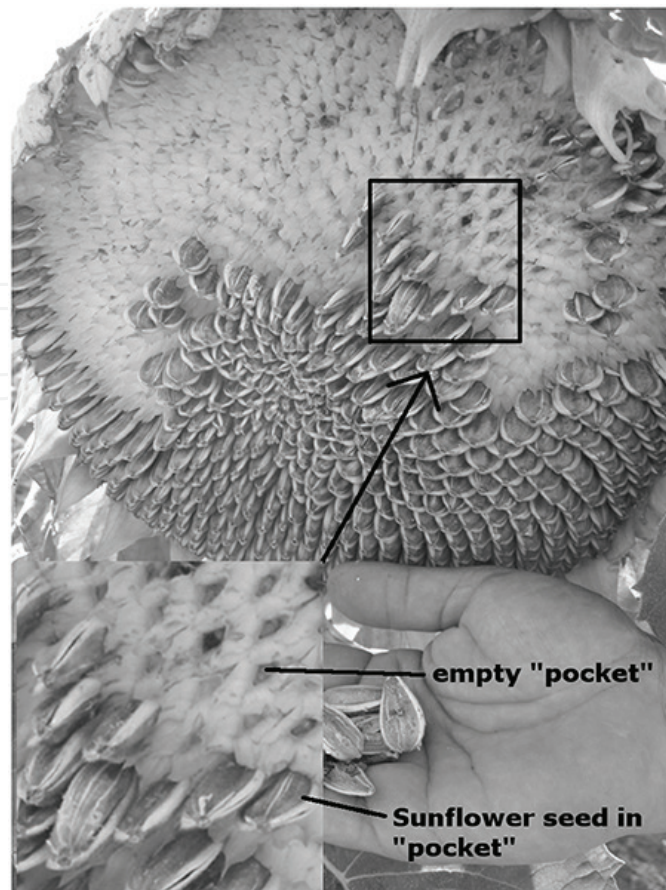


Figure 7. Left: points of interest detected in an image of a sunflower field.

This view clearly shows the Hessian-detecting characteristics. Medium: Warp types applied in SURF. Right: Image of graffiti showing the size of the window descriptors on different scales.

The first levels of each Octavian are relatively large. **Figure 7** (left) shows the points of interest detected when quick-Hessian detection is applied.

6. SURF description

The superior performance of SIFT compared with that of other [9] benchmarks is remarkable. Their mixing with local informatics and the distribution of gradient-related characteristics provide fine characteristic resistance that mitigates the effect of settlement faults in terms of size or surface area. The application of relative resistance and gradient directions decreases the effect of illumination changes. The proposed SURF descriptor is based on similar properties, further complicating the process. The first step is to identify a direction that can be reproduced from data from a circular area surrounding the indicator of interest. Next, we

construct a square area aligned with a specific orientation and extract the description from it. In addition, we also offer a vertical version number of our descriptor (U-SURF), which is not fixed for in image rotation and rapidly calculates and improves camera location.

6.1. Orientation assignments

To fix the rotation, we define a reproducibility orientation for points of interest. To this end, we first compute the Haars wavefunction that corresponds to the X and Y direction. It is located in a boundary with a radius vector $7s$ surrounding the indicator of interest, with the image being detected as the point of interest. The sampling step depends on the scale and its selection is s . Wavelet responses are also computed in the current range s . Thus, the size of the wavelet on a large scale is also large. We therefore use the integrated image as a quick filter. Only seven operations are required for SURF to calculate the corresponding Z or Y direction at any scale. The lateral distance of the wavelength is $4s$. Once the responses are calculated and weighed with Gaussians ($\sigma = 2.51s$) centered around the indicators of interest, the responses are represented as vectors in range with the horizontal angle corresponding to force alongside the output and the vertical angle corresponded to the force along the coordinate. The trend is estimated by calculating the amount of all responses in navigation windows with an angle of $\pi/3$. The horizontal and vertical angle responses are summarized in the windows. The synthesized questionnaires then produce new vectors. The long vectors of its kind are directed towards the indicator of interest. The range of the slide windows is the argument, which was chosen empirically. Smaller sizes focus on one dominant, maximizing yield size in vectorial lengths that are not expressive. Both lead to an unstable trend in the area of interest. Note that U-SURF skips over this step.

6.2. Description component

To extract a description, a window centered around the indicator of interest must be constructed. The area must be oriented in the direction specified in the previous section. This transformation is unnecessary for a vertical copy. The size of this window is $20s$. The area is regularly divided into small 4×4 subregions to preserve crucial data in each subregion. We calculate some simple characteristics in a 5×5 regularized subregion. For simplification, we designated the DEX response waveform Haars in the horizontal direction and colored the prepared Haars corresponding to the vertical angle direction (2S filters size). Here, the terms "horizontal" and "vertical" are defined with respect to the orientation of the specified point of interest. To increase robustness to geometrical distortions and localization faults, the DEX and dy responses are first weighted with a Gaussian ($\sigma = 3.4s$) centered around the indicator of interest. Then, the wavelength and dz. and dy wavelet responses are summarized above each subregion and are the first place of inputs in the vectorial function. To provide data on changes in polarity density, we also extract total absolute value for the replay of $|dz|$ and $|dy|$. Thus, each sub region has a four-dimensional descriptor for the underlying intentional structure that leads to a vectorial description of all 4×4 sub regions of distance 64. Wavelength response is constant to polarize the illuminated "offset." Contrast (factor range) is obtained by converting the description into a vector unit. The characteristics of three different image

intensities in a subregion. Imaging groups of these general density models can be applied to produce a distinct description. To access the SURF descriptor, we experimented by subtracting and adding waves, applying d_2z and d_2y , adding first-order waves, applying PCA, and identifying the intermediate and average values. From a comprehensive evaluation, the outer part performs best among all parts (Figure 8).

$$\mathbf{v} = (\sum d_x, \sum d_y, \sum |d_x|, \sum |d_y|) \tag{6}$$

Left: the state of a homogeneous zone. All values are relatively small. Center: in the presence of frequency in the direction of z , the value $\sum |d_x|$ increases but remains low. If the density increases progressively in the direction of x , the two values $\sum d_x$ and $\sum |d_x|$ increase.

We change the sampling count for indicators and subfields. A sampling subregion of 4×4 provides good results. Given the fine divisions, it appears to be less powerful, significantly increasing the timing of correspondence. In other methods, the shortage circuit with 3×3 subregions (SURV-35) provides poor results but allows for rapid computation and is relatively acceptable compared with other descriptors in the literature. Figure 9 shows just some of the compared results (SURV-126 will be explained soon).

The two different match strategy tests performed on the "Graffiti" image with width changes of 30 points from the current description. Points of interest are calculated through the "Quick Hessian" detection method. Note that rates are unfixed per affine. Therefore, the results are not identical to those of [9]. Surf-126 corresponds to the expanded description. Left: similarity between threshold element and match strategy. Right: strategy for closer contact.

We test another section of the SURF descriptor by adding two similar characteristics (SURV-126). It repeatedly uses the same quantities as before but has additional divisors. The values of dz and $|dz|$ are calculated individually for $dy < 0$ and $dy \geq 0$. Likewise, the values of dy and $|dy|$ are separate and agree with the signal of dz , thereby duplicating the count of the feature. Description is more distinct and does not require long computation time. However, matching time is slow because of the high dimensions of the features. The argument choice is equated for the "Graffiti" sequence [9] because it contains out-of-play rotation in the rotation map, as well illumination changes. The general description of 4×4 sub regions (SURF-126) improves

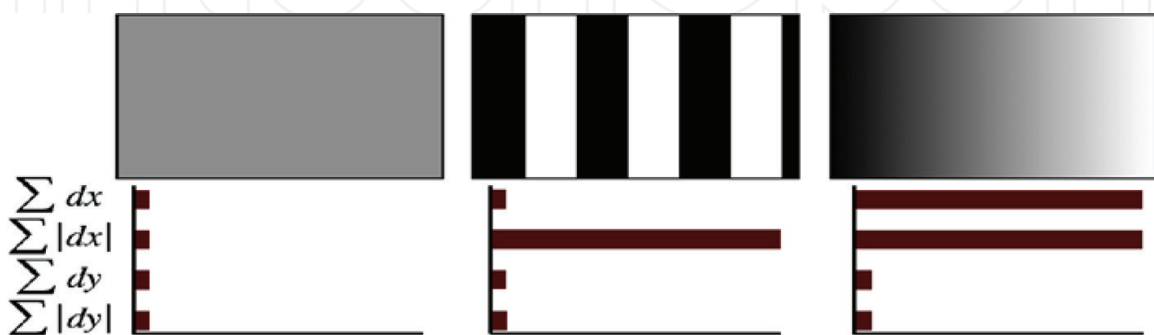


Figure 8. Descriptive entries for a subregion representing the universal base density model.

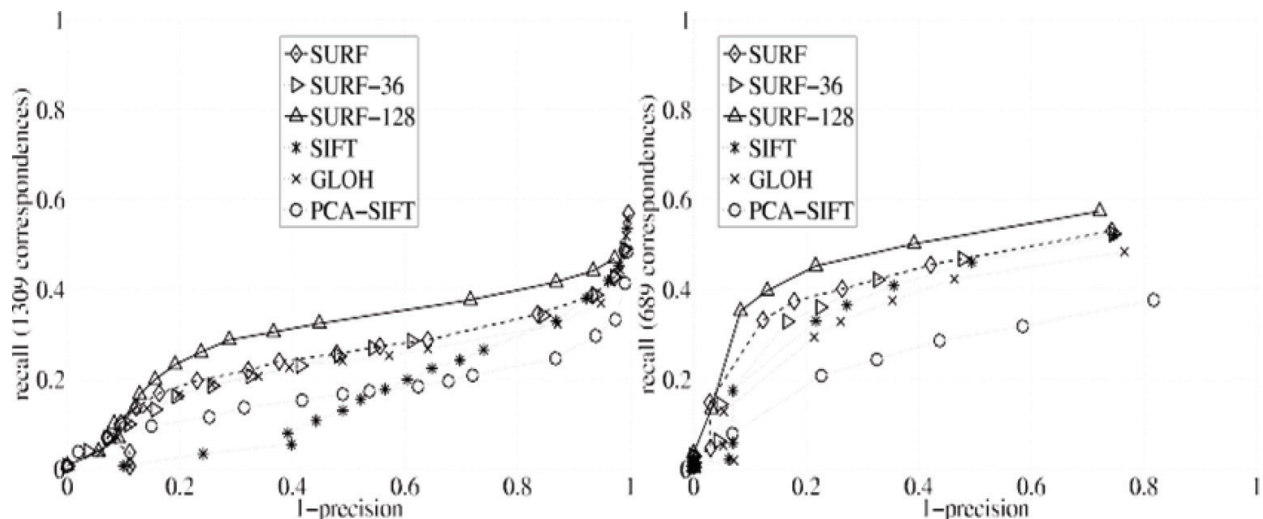


Figure 9. Line graphs for different methods.

performance. In addition, SURF has excellent performance that surpasses that of the latest state-of-the-art algorithm. To provide an index of the pairing phase, Laplacian signs (i.e., the Hessian matrix effect) are included for the basic point of interest. Typically, the points of interest are in plug-type structures. The label marks luminous points on the darker background of the reversed situation. This functionality is available at an additional price, which has already been calculated throughout the detecting process. During matching, we compare the feature only if they have the similar contrast types. Thus, this minimum data speeds up matching and improves performance.

7. Experimental results

We provide solutions for a standard evaluation set without detection and description. Then, we discuss the solutions obtained during when applying the algorithm to apply the real object. All detectors and descriptions are based on comparison with the original application of the authorizer. In standard evaluation, we test our detectors and describe the applied sequence of images and software tests. The test set included images of actual, narrow, and structured scenes. Given the limited page count of this manuscript, we cannot provide the results of all sequences. To compare the performances of the detectors, we selected images with changes in perspective (Graffiti and Wall), magnification and rotation (Boats), and illumination (Leuven). Test notes for all sequences are presented in addition to the base sequence. We applied the degree of repetition, as described in [10], to detect the number of points of interest in two images relative to the indicator of interest (which is only the visible part of both images). The performance of the detection algorithm was compared with that of the Gaussian (DOG) [2], Harris, and Hessian Laplace [12] algorithms. All algorithms provided similar number of points of interest. This finding applies to all images, including the database used in the object recognition experiment (see **Table 1** for an example). In addition,

Detecting	Threshold	Nb of indicators	Compu. time (ms)
Quick Hessian	601	1417	119
Hessian-Laplace	900	1980	651
Harris-Laplace	2400	1665	1799
DoG	Default	1521	401

Table 1. Threshold element, numbers of points detected, and computational time (the first image of the graffiti sequence, 900×640).

the computational speed of our Quick Hessian detector was more than three times faster than that of DOG and five times quicker than that of Hessian Laplace. At certain timepoints, the repetitions of our detector approximated (Graffiti, Leuven, Boat) or exceeded (Walls) that of the competition. The Graffiti and Walls sequences contained out-of-play gyration, and solutions in affine contortions when the detection compared only gyration and were scaled invariantly. Therefore, distortions must be addressed through the overall durability of features. The descriptors were evaluated by the applied call diagrams (1 precisely) in [3, 9]. In each evaluation, we applied the first and fourth images of the sequence, except for the Graffiti image and the Walls scenario. The corresponding perspective change was 30 and 50 points., we compared our SURF signifier (GLOH0, SIFT, and PCA-SIFT) with our “Quick Hessian” detector. SURF outperformed the other signifiers in almost all tests. In **Figure 4**, we equated the solutions applied to two different corresponding techniques— one established on the same threshold element and one founded on the closest neighbor proportion (see [9] for a discussion of this technique). This phenomenon affected the order of descriptors but SURF performance is better in both events because of limited spacing. However, the only solutions on likeness similar to the similarity threshold are shown in **Figure 7** because this technique is most appropriate for representing the runner distribution in its advantage spacing [9] and used more routinely. SURF descriptor is systematically and extensively superior to other descriptors and exhibited 11% improvement. Its computational time is rapid (**Table 2**). The microprocessor (Surf-126) seems to be slightly superior to the general SURF system. However, its matching process was slow. Thus, it may be unsuitable for applications that require speed. Object recognition was performed under a similar set of standards and threshold element (**Table 1**). The moment was evaluated on a standard Unix computer (Pentium IV, 2.5GHZ). The objects are recognized because we experienced new

	U-SURF	SURF	SURF-126	SIFT
Time (ms)	254	355	390	1035

The threshold element is adjusted to detect the same number of indicators of interest for all methods. The relatively shorter calculation time also represents the other image.

Table 2. Calculation time for common detectors—descriptive applications, testing on the first image of the Graffiti sequence.



Figure 10. Example images of the reference group (left) and the test group (right). Note the difference in perspective and colors.

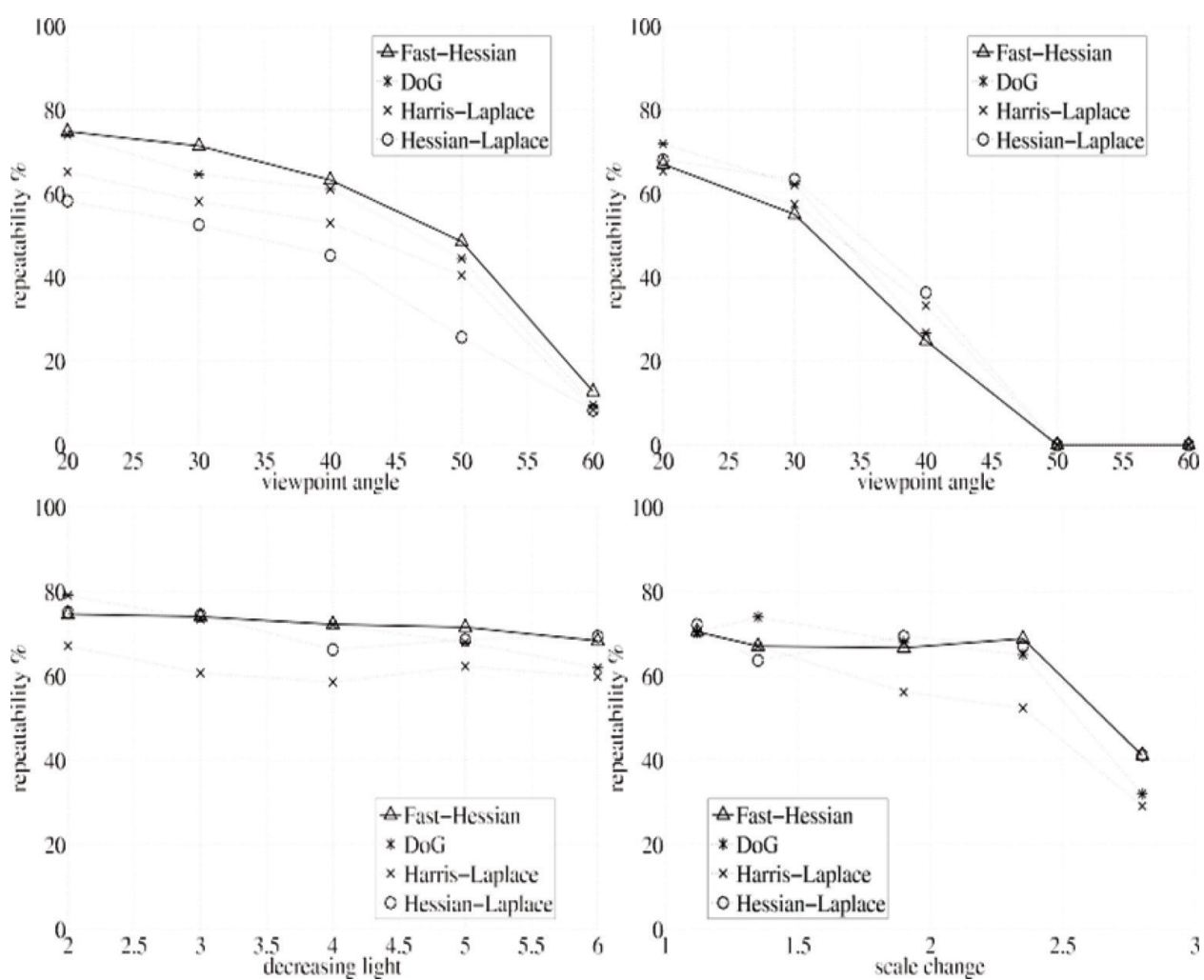


Figure 11. Left to right and from top to bottom: Frequency of Walls-Graffiti (perspective change), Leuven (illumination change), and Boats (magnification and rotation).

functionalities on the practical application, aiming to identify the art object in the museum. The data consisted of 216 images of 22 objects. The test group images comprised 116 images.

Under different conditions, including extreme illumination changes, object reflections in glass cabinetry, changes in perspective, magnification, and differences in camera quality, images are small (319×240) and difficult to recognize because they lose detail. To identify the objects in the database management, we proceed as follows: The images of the test group are compared with all the images of the reference group by associating their respective indicators of interest. The object represented on the reference image is selected with the greatest amount of correspondence with respect to the test image as a recognized object. Correspondence is performed as follows: A perspective of interest in the test image is compared with a perspective of interest in the referenced image by computing the value of Euclidean space between the vector and its descriptors. A corresponding pair is detected if the vision distance is closer by 0.6 times than that from the closest neighbor to the second. It is the closest strategy that corresponds to the ratio of the neighbors [2, 8, 27]. Extra engineering restrictions reduced the impact of false-positive matching, and this can be performed over any situation. For comparative reasoning, this does not make sense because it may be hiding the lack of the basic tables. On average, the rating reflection of the solutions of our performed appraisal is established. The leaders are SURF-126 with a recognizability rate of 85.7%, followed by U-SURF (84.8%), and SURF (83.7%). The other descriptors were 78.4% for GLOH, 78.2% for SIFT, and 72.3% for PCA-SIFT (Figures 10 and 11).

8. Discussion and conclusions

A brain-computer interface (BCI) is a direct interface between the human brain and an artificial system. Its purpose is to control the actuation of a device.

Many researchers have proposed modern algorithms to solve the problem of image authentication. This study explored and compared the application of different algorithms that detect common types of image forgery. The characteristics of the algorithms are shown in **Table 2**. The algorithms we examined in this study are undoubtedly important for the detection of image counterfeiting. Previous researchers have attempted to improve the reliability of image fraud detection algorithms. They have achieved this objective by (1) reducing algorithm complexity and computational time. This objective was achieved by using small vector dimensions, as shown in Refs. [18, 37–41] increasing the robustness of the algorithms. This aim was achieved by adopting a powerful feature that is consistent for a wide range of image processes, as shown in Refs. [42–48]. The algorithm based on fixed key indicators and fixed instances exhibits remarkable performance, as shown in **Table 2**. However, several barriers and challenges remain. We summarize the defects of available algorithms in **Tables 1** and **2**: (1) the algorithms cannot handle all possible types of image processing that can be applied to forge images; (2) some algorithms rely heavily on several threshold elements or initial value, and the identification of these threshold elements and values require experimentation and improvements; and (3)

most current methods take time [49, 50]. The development of complex and reliable algorithms that quickly and rapidly detect image forgery has been proposed. However, future work must overcome the following challenges: (1) the lack of standardized datasets for false counterfeiting limits the comparability and reproduction of existing algorithms, as well the design of improved algorithms and (2) the lack of common quantitative methods for measuring and evaluating algorithm performance prevents the comparison of different algorithms under different conditions. We believe that this reason accounts for the absence of studies that compare

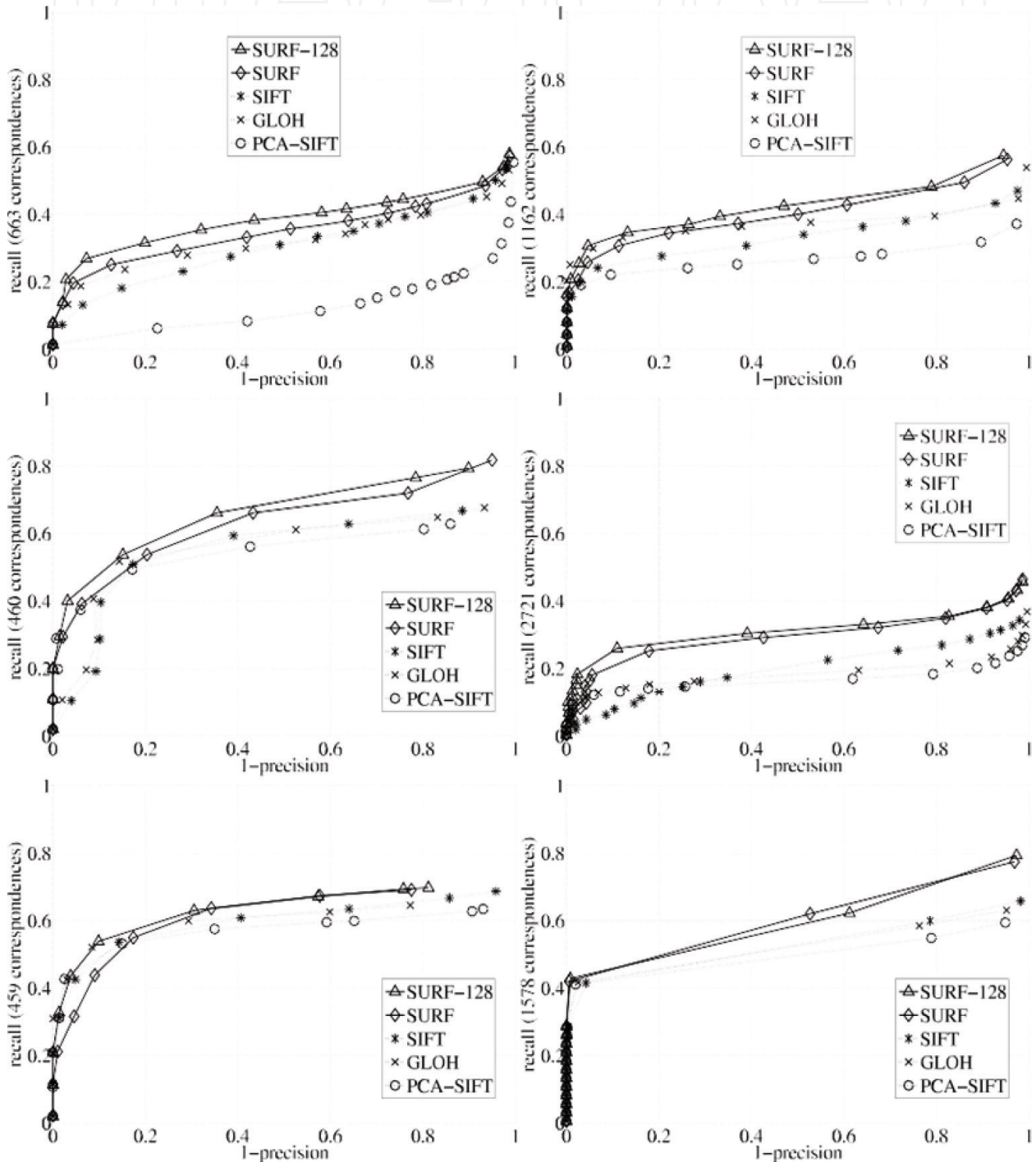


Figure 12. Left to right and top to bottom: graphs of changes in 50 (Walls) grades, descale element 2 (Boats), image blur (Bikes and Trees), illumination level (Leuven), and JPEG compression (Ubc).

the accuracy and performance of different algorithms. Given that detecting counterfeiting is still in its early stages, considerable work remains to be performed, and other ideas can be derived or borrowed from other fields, such as object recognition or image analysis (**Figure 12**).

Author details

Haitham Hasan Badi^{1*}, Bassam Sabbri² and Fitian Ajeel²

*Address all correspondence to: haitham@uoitc.edu.iq

1 Information of Computer Science and Information Technology, University of Malaysia, Kuala Lumpur, Malaysia

2 University of Information Technology and Communication, Baghdad, Iraq

References

- [1] Ho A, Shi Y, Kim H, Barni M, Wang W, Dong J, Tan T. A survey of passive image tampering detection. In: Digital Watermarking. Vol. 5703. Berlin/Heidelberg: Springer; 2009. pp. 308-322
- [2] Liu G, Wang J, Lian S, Wang Z. A passive image authentication scheme for detecting region-duplication forgery with rotation. *Journal of Network and Computer Applications*. 2010;**34**(5):1557-1565
- [3] Sebe N, Liu Y, Zhuang Y, Huang T, Chang S-F. Blind passive media forensics: Motivation and opportunity. In: *Multimedia Content Analysis and Mining*. Vol. 4577. Berlin/Heidelberg: Springer; 2007. pp. 57-59
- [4] Hu J, Zhang H, Gao Q, Huang H. An improved lexicographical sort algorithm of copy-move forgery detection. In: *Proceedings—2nd International Conference on Networking and Distributed Computing, ICNDC 2011*. 2011. pp. 23-27
- [5] Bo X, Junwen W, Guangjie L, Yuewei D. Image copy-move forgery detection based on SURF. In: *International Conference on Multimedia Information Networking and Security (MINES)*. 2010. pp. 889-892
- [6] Lian S, Kanellopoulos D. Recent advances in multimedia information system security. *Informatica*. 2009;**33**:3-24
- [7] Rey C, Dugelay J-L. A survey of watermarking algorithms for image authentication. *EURASIP Journal on Applied Signal Processing*. 2002;**2002**(1):613-621
- [8] Kundur D, Hatzinakos D. Digital watermarking for telltale tamper proofing and authentication. In: *Proceedings of the IEEE*. Vol. 87. 1999. pp. 1167-1180
- [9] Zhou L, Wang D, Guo Y, Zhang J. Blur detection of digital forgery using mathematical morphology. In: *Proceedings of the 1st KES International Symposium on Agent and Multi-Agent Systems: Technologies and Applications*. Wroclaw, Poland: Springer-Verlag; 2007

- [10] Redi JA, Taktak W, Dugelay JL. Digital image forensics: A booklet for beginners. *Multimedia Tools and Applications*. 2011;51(1):133-162
- [11] Ardizzone E, Bruno A, Mazzola G. Copy-move forgery detection via texture description. In: *MiFor'10—Proceedings of the 2010 ACM Workshop on Multimedia in Forensics, Security and Intelligence, Co-located with ACM Multimedia 2010*. 2010. pp. 59-64
- [12] Kang L, Cheng XP, Li K, Xiao-ping C. Copy-move forgery detection in digital image. In: *Image and Signal Processing (CISP)*. 2010 3rd International Congress. Vol. 5. 2010. pp. 2419-2421
- [13] Ryu SJ, Lee MJ, Lee HK. Detection of copy-rotate-move forgery using zernike moments. In: *Lecture Notes in Computer Science (Including Subseries Lecture Notes in Artificial Intelligence and Lecture Notes in Bioinformatics)*. LNCS. Vol. 6387. 2010. pp. 51-65
- [14] Lowe DG. Object recognition from local scale-invariant features. In: *Proceedings of the IEEE International Conference on Computer Vision*. Vol. 2. 1999. pp. 1150-1157
- [15] Bay H, Tuytelaars T, Van Gool L. SURF: Speeded up robust features. In: *Lecture Notes in Computer Science (Including Subseries Lecture Notes in Artificial Intelligence and Lecture Notes in Bioinformatics)*. LNCS. Vol. 3951. 2006. pp. 404-417
- [16] Huang H, Guo W, Zhang Y. Detection of copy-move forgery in digital images using sift algorithm. In: *Proceedings—2008 Pacific-Asia Workshop on Computational Intelligence and Industrial Application*. PACIIA 2008. Vol. 2. 2008. pp. 272-276
- [17] Ardizzone E, Bruno A, Mazzola G. Detecting multiple copies in tampered images. In: *Proceedings—International Conference on Image Processing, ICIP*. 2011. pp. 2117-2120
- [18] Zhang C, Guo X, Cao X. Duplication localization and segmentation. In: *Lecture Notes in Computer Science (Including Subseries Lecture Notes in Artificial Intelligence and Lecture Notes in Bioinformatics)*. LNCS No. Part 1. Vol. 6297. 2010. pp. 578-589
- [19] Amerini I, Ballan L, Caldelli R, Del Bimbo A, Serra G. A SIFT-based forensic method for copy-move attack detection and transformation recovery. *Information Forensics and Security, IEEE Trans*. 2011;6(3):1099
- [20] Pan X, Lyu S. Detecting image region duplication using SIFT features. In: *Acoustics Speech and Signal Processing (ICASSP), 2010 IEEE International Conference*. 2010. pp. 1706-1709
- [21] Pan X, Lyu S. Region duplication detection using image feature matching. *IEEE Transactions on Information Forensics and Security*. 2010;5(4):857-867
- [22] Shivakumar BL, Baboo S. Automated forensic method for copy-move forgery detection based on Harris interest points and SIFT descriptors. *International Journal of Computer Applications*. 2011;27(3):9-17
- [23] Shamshiri F. Rotten Gods [Online]. 2008. Available: <http://www.rottenegods.com/2008/07/missles-forgery.html> [Accessed 01.03.12]
- [24] Ng T-T, Chang S-F. A model for image splicing. In: *International Conference on Image Processing (ICIP 04)*. Vol. 2. 2004. pp. 1169-1172

- [25] Dong J, Wang W, Tan T, Shi YQ. Run-length and edge statistics based approach for image splicing detection. In: *Lecture Notes in Computer Science (Including Subseries Lecture Notes in Artificial Intelligence and Lecture Notes in Bioinformatics)*. LNCS. Vol. 5450. 2009. pp. 76-87
- [26] Zhen F, Shuozhong W, Xinpeng Z. Image splicing detection using color edge inconsistency. In: *Multimedia Information Networking and Security (MINES), 2010 International Conference*. 2010. pp. 923-926
- [27] Christlein V, Riess C, Angelopoulou E. On rotation invariance in copy-move forgery detection. In: *IEEE International Workshop on Information Forensics and Security, WIFS*. 2010
- [28] Wang X, Zhang X, Li Z, Wang S. A DWT-DCT based passive forensics method for copy-move attacks. In: *2011 Third International Conference on Multimedia Information Networking and Security*. 2011. pp. 304-308
- [29] Cao Y, Gao T, Fan L, Yang Q. A robust detection algorithm for region duplication in digital images. *International Journal of Digital Content Technology and its Applications*. 2011; 5(6):95-103
- [30] Cao Y, Gao T, Fan L, Yang Q. A robust detection algorithm for copy-move forgery in digital images. *Forensic Science International*. 2011
- [31] Huang Y, Lu W, Sun W, Long D. Improved DCT-based detection of copy-move forgery in images. *Forensic Science International*. 2011;3:178-184
- [32] Myrna AN, Venkateshmurthy MG, Patil CG. Detection of region duplication forgery in digital images using wavelets and log-polar mapping. In: *Conference on Computational Intelligence and Multimedia Applications, 2007, International Conference*. Vol. 3. 2007. pp. 371-377
- [33] Bravo-Solorio S, Nandi AK. Automated detection and localisation of duplicated regions affected by reflection, rotation and scaling in image forensics. *Signal Processing*. 2011; 91(8):1759-1770
- [34] Bravo-Solorio S, Nandi AK. Passive forensic method for detecting duplicated regions affected by reflection, rotation and scaling. In: *17th European Signal Processing Conference (EUSIPCO 2009)*. 2009. pp. 824-828
- [35] Bayram S, Sencar HT, Memon N. An efficient and robust method for detecting copy-move forgery. In: *Proceedings of IEEE International Conference on Acoustics, Speech and Signal Processing*. 2009. pp. 1053-1056
- [36] Li W, Yu N. Rotation robust detection of copy-move forgery. In: *Proceedings—International Conference on Image Processing, ICIP*. 2010. pp. 2113-2116
- [37] Lin H-J, Wang C-W, Kao Y-T. Fast copy-move forgery detection. *WSEAS Transactions on Signal Processing*. 2009;5(5):188-197
- [38] Ardizzone E, Mazzola G. Detection of duplicated regions in tampered digital images by bit-plane analysis. In: *Lecture Notes in Computer Science (Including Subseries Lecture*

- Notes in Artificial Intelligence and Lecture Notes in Bioinformatics). LNCS. Vol. 5716. 2009. pp. 893-901
- [39] Tamura H, Mori S, Yamawaki T. Textural features corresponding to visual perception. *IEEE Transactions on Systems, Man, and Cybernetics*. 1978;**8**(6):460-473
- [40] Jain AK, Farrokhnia F. Unsupervised texture segmentation using Gabor filters. *Pattern Recognition*. 1991;**24**(12):1167-1186
- [41] Haralick RM. Statistical and structural approaches to texture. *Proceedings of the IEEE*. 1979;**67**(5):786-804
- [42] Fridrich J, Soukal D, Lukáš J. Detection of copy-move forgery in digital images. In: *Proceedings of DFRWS 2003*. USA: Cleveland, OH; 2003
- [43] Wu Q, Wang S, Zhang X. Detection of image region-duplication with rotation and scaling tolerance. In: *Lecture Notes in Computer Science (Including Subseries Lecture Notes in Artificial Intelligence and Lecture Notes in Bioinformatics)*. LNAI. Vol. 6421. 2010. pp. 100-108
- [44] Wu Q, Wang S, Zhang X. Log-polar based scheme for revealing duplicated regions in digital images. *IEEE Signal Processing Letters*. 2011;**18**(10):559-562
- [45] Penatti OAB, Valle E, da R, Torres S. Comparative study of global color and texture descriptors for web image retrieval. *Journal of Visual Communication and Image Representation*. 2012;**23**(2):359-380
- [46] Van De Sande K, Gevers T, Snoek C. Evaluating color descriptors for object and scene recognition. *IEEE Transactions on Pattern Analysis and Machine Intelligence*. 2010; **32**(9):1582-1596
- [47] Langille A, Minglun G. An efficient match-based duplication detection algorithm. In: *Computer and Robot Vision, 2006. The 3rd Canadian Conference*. 2006. p. 64
- [48] Luo W, Huang J, Qiu G, Weiqi L, Jiwu H, Guoping Q. Robust detection of regionduplication forgery in digital image. In: *Proceedings of the 18th International Conference on Pattern Recognition*. Vol. 04. 2006. pp. 746-749
- [49] Zimba M, Xingming S. Fast and robust image cloning detection using block characteristics of DWT coefficients. *International Journal of Digital Content Technology and its Applications*. 2011;**5**(7):359-367
- [50] Won CS, Park DK, Park S-J. Efficient use of MPEG-7 edge histogram descriptor. *ETRI Journal*. 2002;**24**(1):23-30